PHYSICAL REVIEW B **86**, 241401(R) (2012)

Effects of strain on band structure and effective masses in MoS_2

H. Peelaers* and C. G. Van de Walle
Materials Department, University of California, Santa Barbara, California 93106-5050, USA
(Received 5 November 2012; published 10 December 2012)

We use hybrid density functional theory to explore the band structure and effective masses of MoS_2, and the effects of strain on the electronic properties. Strain allows engineering the magnitude as well as the nature (direct versus indirect) of the band gap. Deformation potentials that quantify these changes are reported. The calculations also allow us to investigate the transition in band structure from bulk to monolayer, and the nature and degeneracy of conduction-band valleys. Investigations of strain effects on effective masses reveal that small uniaxial stresses can lead to large changes in the hole effective mass.

DOI: 10.1103/PhysRevB.86.241401 PACS number(s): 71.20.Nr, 71.70.Fk, 73.22.−f

Molybdenum disulfide (MoS_2) is a semiconducting material, widely used as a dry lubricant because of its structural similarity to graphite. It consists of stacked hexagonal S-Mo-S layers (Fig. 1). These layers, conventionally referred to as monolayers of MoS_2, are weakly bound by van der Waals forces. Similarly to the production of graphene, MoS_2 samples consisting of a single or a few monolayers can by produced by micromechanical exfoliation[1]—but, contrary to graphene, MoS_2 actually has a band gap. Monolayer MoS_2 field-effect transistors have already been demonstrated,[2] but devices based on multilayers show great promise as well.[3]

Many details about the electronic properties of bulk MoS_2 are still lacking. In this Rapid Communication we report comprehensive results for band structure, addressing direct and indirect band gaps and multiple conduction-band valleys, as well as effective masses. We also investigate how strain affects these properties, in the process also clarifying the differences in band structure between bulk and monolayer. Strain effects on monolayers and bilayers have already been investigated,[4,5] but results for bulk MoS_2 are not yet available. Strain can result from externally applied stress, or arise from pseudomorphic growth[6–8] or when a MoS_2 layer is clamped to a substrate. We quantify the changes in the band structure as a function of strain in terms of deformation potentials. All of the quantities reported here are relevant for further development of electronic applications of this material as well as for device modeling.

We investigate the two types of deformations that are relevant for MoS_2: uniaxial and biaxial. Uniaxial strain parallel to the c direction, which we denote by ε_{zz}, directly affects the interlayer separation. In the limit of large tensile strain, interlayer distances become large and interactions negligible, and we effectively reach the monolayer limit. Thus the investigation of the effects of tensile uniaxial strain provides insight into the transition between the bulk system and the monolayer. We impose a given value of the c lattice parameter, corresponding to a given ε_{zz}, and allow for a relaxation of the lattice parameters in the perpendicular direction, as would occur in a realistic uniaxial stress geometry. For biaxial stress, we impose a value of the in-plane lattice parameters a (or equivalently b), corresponding to a strain $\varepsilon_{xx} = \varepsilon_{yy}$. In this case we also allow for lattice relaxation in the direction parallel to c, corresponding to biaxial stress.

All calculations are based on generalized Kohn-Sham theory with the screened hybrid functional of Heyd, Scuseria, and Ernzerhof (HSE06, Ref. 9) and the projector augmented-wave (PAW) pseudopotential plane-wave method[10] as implemented in the VASP code.[11] For the PAW pseudopotential for Mo we included the full $n = 4$ shell ($4s^2$, $4p^6$, and $4d^5$) plus $5s^1$ as valence. For S, the $n = 3$ shell is included as valence ($3s^2$ and $3p^4$). A $10 \times 10 \times 2$ Monkhorst-Pack[12] **k**-point grid was used for all calculations and a plane-wave basis set with an energy cutoff of 280 eV.

The hybrid functional approach is well suited to describe both structural properties and band structures,[13] in particular the band gaps of semiconductors, which are severely underestimated when using standard exchange-correlation functionals such as the local-density approximation (LDA) or the generalized gradient approximation (GGA). van der Waals interactions, which govern the interlayer distance in MoS_2, are not explicitly included in HSE06; in fact, this is still an area of active research within density functional theory. We therefore fix the c lattice parameter (which is overestimated by 5.6% in HSE06) to its experimental value (12.29 Å, Ref. 14), a practice also applied in previous computational studies.[15,16]

Table I compares our calculated band gaps of bulk MoS_2 with previously published values. Bulk MoS_2 is an indirect-band-gap material, with the valence-band maximum (VBM) located at the Γ point and the conduction-band minimum (CBM) at a point on the Γ-K line; we denote this minimum as $\Lambda_{\min}$ [see Fig. 1(c)]. We also examine the direct K-K band gap. Both LDA and GGA underestimate the band gaps. In the GW_0 method[17] the one-electron Green's function G is self-consistently updated, while the screened Coulomb interaction W is fixed at its initial value. QSGW stands for the quasiparticle self-consistent GW method utilized in Ref. 16. The GW methods slightly underestimate the indirect band gap, but overestimate the direct gap. Our approach based on the HSE06 functional slightly overestimates the gaps compared to experiment—though we note that the optically measured gaps probably reflect excitonic contributions that are not included in our calculations. Overall, this comparison confirms that the hybrid functional is the right choice for our study, since in addition to providing band structures of comparable or better quality than those obtained with other approaches, it allows calculating forces (not available in the GW approaches), needed to relax the system in response to applied stresses.

Figure 2 shows the calculated band structure for different values of uniaxial stress along the c direction. The

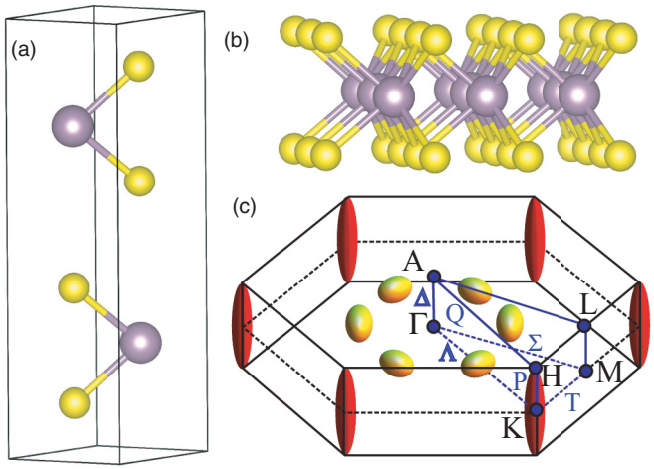

FIG. 1. (Color online) (a) Side view of the bulk unit cell of MoS_2. (b) A monolayer of MoS_2. (c) The hexagonal Brillouin zone. High symmetry points and lines are indicated. The conduction-band valleys at Λ_{min} and K are schematically depicted, with ellipsoids representing constant-energy surfaces.

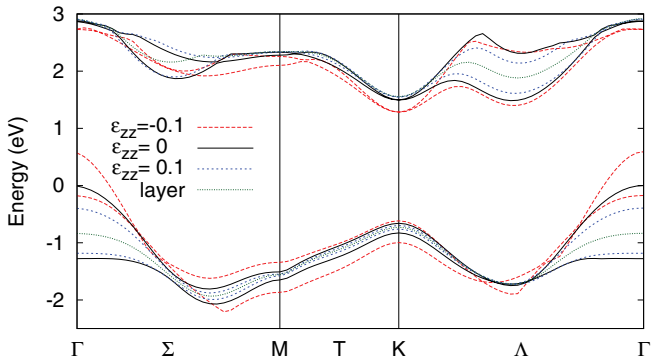

FIG. 2. (Color online) Band structure of bulk MoS_2 under uniaxial stress along the c axis, plotted along high-symmetry lines in the in-plane Brillouin zone. The band structure of unstrained bulk and an unstrained monolayer are also shown. For clarity we only show the highest two valence bands and lowest two conduction bands. The labels underneath the segments of the Brillouin zone indicate the names of the high-symmetry lines [see Fig. 1(c)].

valence-band maximum (VBM) of the bulk is chosen as the zero energy reference, and the band structures are aligned using the Mo 4s electrons as reference states. Since we are interested in a comparison with the monolayer and in transport within the layers, we focus on the in-plane part of the Brillouin zone.

As noted above, bulk MoS_2 has an indirect band gap Γ-Λ_{min}. The monolayer, on the other hand, has a direct band gap, located at the K point. As the layers are moved apart (corresponding to an increase in ε_{zz}), a transition from the indirect band gap to the direct gap occurs, but only when the interlayer distance is increased by almost 50%. As seen in Fig. 2, the VBM at Γ moves down in energy, while the VB shift at the K point is much smaller. The location of the VBM thus shifts from Γ to K. Simultaneously the Λ_{min} CBM moves higher in energy compared to the K point, shifting the overall minimum to the K point. The switch of location of the CBM occurs for much smaller strains than the switch of the VBM. Therefore, with increasing tensile strain the nature of the band gap switches from indirect Γ to Λ_{min}, via indirect Γ to K, to direct K to K, as illustrated in Fig. 3(a).

The relative shift of the VB $-$ 1 and the CB $+$ 1 bands is opposite to that of the highest VB and lowest CB, as these bands originate from the two different S-Mo-S layers that form the bulk unit cell [Fig. 1(a)], and thus have to merge into one degenerate band for large ε_{zz} (large interlayer distance).

For compressive strains ($\varepsilon_{zz} < 0$), the VBM at Γ moves up and the CBM at K moves down; the band gap remains indirect. We note that in unstrained bulk the CBM at Λ_{min} is only slightly higher in energy than the minimum at K, and the energy difference between the Γ-K and Γ-Λ_{min} band gaps remains smaller than 0.02 eV for strains less than 5%. This near degeneracy, along with the multiplicity of these off-Γ CB valleys, is an important feature for device applications since it affects the density of states. The CB valleys are schematically depicted in Fig. 1(c), where the Λ_{min} has a multiplicity of 6 (inner ellipses) and the valley at K a multiplicity of 2 (ellipses at edge, $6 \times 1/3 = 2$).

Our result for a near degeneracy between the Λ_{min} and K CB minima somewhat differs from a previous report based on HSE06 hybrid functional calculations,[15] in which the CB at K was found to be ~0.3 eV higher in energy than at Λ_{min}. Possible reasons for the discrepancy could be the use of a different basis set (Gaussians versus plane waves) or the use of pseudopotentials versus PAWs. This can also be seen in Table I, where the direct band gap (from K to K) differs in magnitude between our approaches. We note that our results are in good agreement with the quasiparticle self-consistent GW results of Ref. 16.

A similar study can be performed for biaxial stress, where now the c lattice parameter is allowed to relax in response to an applied in-plane strain. The biaxial stress results are shown in Fig. 3(b); we used the data from Fig. 3(a) to correct for the difference between the calculated and experimental values of the c lattice parameter. Figure 3(b) shows that for positive (tensile) strain the CBM at Λ_{min} shifts up, and the CB at

TABLE I. Band-gap energies (in eV) for bulk MoS_2 calculated using different methods.

	LDA	GGA	HSE06	HSE06[a]	GW_0[b]	QSGW[c]	Experiment[d]
Indirect	0.81	0.86	1.48	1.48	1.23	1.29	1.29
Direct	1.80	1.58	2.16	2.33	2.07	2.10	1.95

[a]Reference 15.
[b]Reference 17.
[c]Reference 16.
[d]Reference 18.

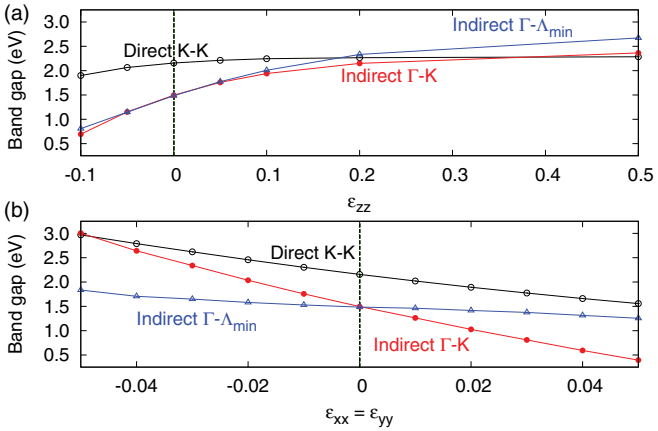

FIG. 3. (Color online) Band gaps of MoS_2 as a function of strain for (a) uniaxial stress along c and (b) biaxial (in-plane) stress. The various gaps are indicated by the locations in the Brillouin zone where the VB and CB extrema occur: indirect Γ-to-$\Lambda_{\min}$ and Γ-to-K gaps, and direct K-to-K gap. The vertical dashed lines indicate unstrained MoS_2.

K shifts down. The VBM remains at Γ. The band gap thus remains indirect for all biaxial stress conditions, switching from Γ to $\Lambda_{\min}$ to Γ to K at a very small tensile strain.

The variation of band gaps with strain can be expressed in terms of deformation potentials, which are useful quantities for device modeling. For small strains in the vicinity of the equilibrium lattice parameters the variation of the gaps is approximately linear, and hence can be expressed as

$$\Delta E_g^{\Gamma\text{-}K} = D_{zz}^{\Gamma\text{-}K}\varepsilon_{zz} \quad \text{and} \quad \Delta E_g^{\Gamma\text{-}K} = D_{\perp}^{\Gamma\text{-}K}(\varepsilon_{xx}+\varepsilon_{yy}), \quad (1)$$

where the second deformation potential is expressed with respect to the sum of the in-plane strains, in analogy with the definition of the deformation potentials D_2 and D_4 in a hexagonal system.[19] Similar expressions hold for the Γ-to-$\Lambda_{\min}$ and K-to-K gaps.

The calculated deformation potentials are listed in Table II. The range over which the linear approximation inherent in Eq. (1) is valid is larger for biaxial strains than in the uniaxial case (see Fig. 3); for the latter, a change in c by 5% changes the deformation potentials by as much as 1 eV.

Note that Eq. (1) is formulated in terms of strain, not stress, and hence the deformation potentials are calculated by varying only the c lattice parameter (in the case of D_{zz}), with the a and b lattice parameters fixed to their equilibrium values. To obtain the variations under uniaxial or biaxial stress conditions that were depicted in Fig. 3, strains along directions parallel as well as perpendicular to c need to be taken into account.

TABLE II. Band-gap energies and deformation potentials (in eV) for uniaxial (along c) and biaxial (in-plane) strains, as defined in Eq. (1).

	E_{gap} (eV)	D_{zz} (eV) (uniaxial)	$D_{\perp}$ (eV) (biaxial)
$E_g^{\Gamma\text{-}\Lambda_{\min}}$	1.48	6.32	−0.56
$E_g^{\Gamma\text{-}K}$	1.50	4.68	−11.65
$E_g^{K\text{-}K}$	2.16	0.28	−7.18

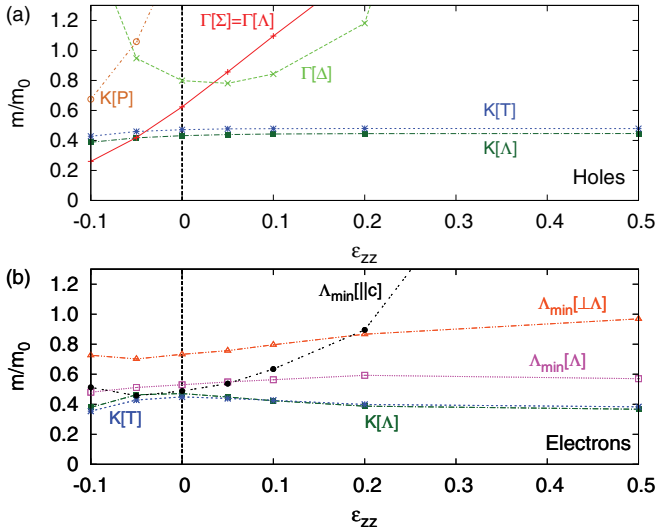

FIG. 4. (Color online) Effective masses (in units of electron mass m_0) for (a) holes and (b) electrons as a function of strain under uniaxial stress conditions. The masses are labeled by the band extremum and (in square brackets) the direction along which the mass is calculated [see Fig. 1(c)]. The vertical dashed line indicates unstrained MoS_2.

Under uniaxial stress, the ratio between ε_{xx} and ε_{zz} is given by Poisson's ratio ν:

$$\varepsilon_{xx} = -\nu\varepsilon_{zz} \quad \text{with} \quad \nu = c_{13}/(c_{11}+c_{12}), \quad (2)$$

where the c_{ij} are the elastic constants of MoS_2. Under biaxial stress, we have

$$\varepsilon_{zz} = -(2c_{13}/c_{33})\varepsilon_{xx}. \quad (3)$$

The combination of Eqs. (1) and (2) or (3) then leads to the results shown in Fig. 3, at least in the linear regime around the equilibrium lattice parameter. Similarly, hydrostatic pressure

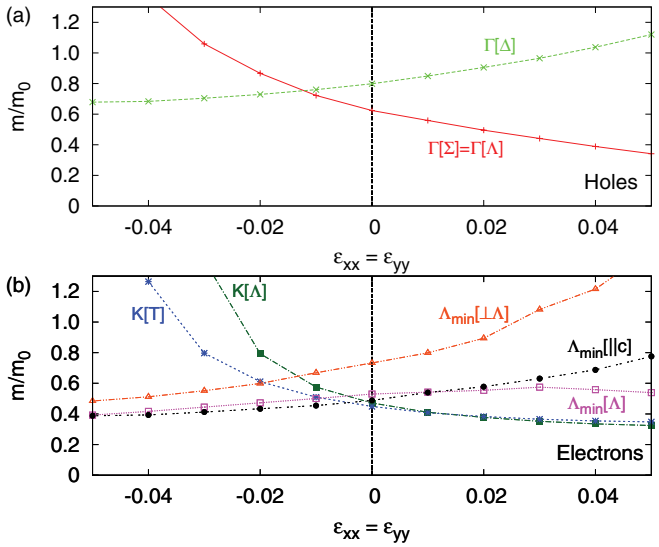

FIG. 5. (Color online) Effective masses (in units of electron mass m_0) for (a) holes and (b) electrons as a function of strain under biaxial stress conditions. The masses are labeled by the band extremum and (in square brackets) the direction along which the mass is calculated [see Fig. 1(c)]. The vertical dashed line indicates unstrained MoS_2.

TABLE III. Effective masses (in units of electron mass m_0) for the unstrained system for bulk and monolayer MoS_2. The masses are labeled by the band extremum and (in square brackets) the direction of the high-symmetry line [see Fig. 1(c)] along which the mass is calculated. Due to the 2D nature, only the in-plane masses are given in the case of the monolayer.

	Hole masses					
	$K[\Lambda]$	$K[T]$	$K[P]$	$\Gamma[\Sigma]=\Gamma[\Lambda]$	$\Gamma[\Delta]$	
Bulk	0.43	0.47	1.73	0.62	0.80	
Monolayer	0.44	0.48		2.80		
	Electron masses					
	$K[\Lambda]$	$K[T]$	$K[P]$	$\Lambda_{min}[\Lambda]$	$\Lambda_{min}[\perp\Lambda]$	$\Lambda_{min}[\|c]$
Bulk	0.47	0.45	>100	0.53	0.73	0.49
Monolayer	0.37	0.38		0.57	0.97	

leads to

$$\varepsilon_{xx} = \varepsilon_{yy} \quad \text{and} \quad \varepsilon_{zz} = \frac{c_{11} + c_{12} - 2c_{13}}{c_{33} - c_{13}} \varepsilon_{xx}. \tag{4}$$

Strain also changes the curvature of the bands, reflected in a change in the effective masses of electrons and holes. Table III reports the effective masses in the unstrained material at the relevant band extrema and along representative high-symmetry directions. Because of the relative weak interaction between layers, we expect out-of-plane masses to be large. This is indeed true in some cases, but not universally: The hole mass at Γ along the Δ direction is only 0.80, and the out-of-plane electron mass at Λ_{min} is only 0.49, of the same order as the in-plane masses.

Figure 4 displays the changes under uniaxial stress. The hole masses for the band extremum at K are not very sensitive to strain, except for the mass along the perpendicular P direction, which increases when the layers are separated. The reason for this is that in the monolayer limit the K and H point become equal. A similar behavior occurs for the other masses in directions perpendicular to the MoS_2 layers, e.g., for the mass at Γ in the Δ direction and at Λ_{min} in the direction parallel to c. For large tensile strains, corresponding to isolated monolayers, the VBM shifts to the K point [see Figs. 2 and 3(a)], but the Γ extremum is the relevant VBM for all experimentally accessible uniaxial stress situations. The mass of the holes at Γ is quite sensitive to strain, and decreases rapidly under compressive uniaxial stress, with values that are identical along the Σ and Λ in-plane directions. For electrons [Fig. 4(b)], the relevant CB extrema are at Λ_{min} and K, and the mass decreases slightly under compressive uniaxial stress.

For biaxial stress (Fig. 5), where we again applied a correction to account for the different c parameter, the Γ hole mass is the same along the Σ and Λ directions and decreases monotonically with increasing in-plane strain. The electron mass at the Λ_{min} CBM exhibits a slow increase with strain, while the electron masses at K decrease with increasing strain. Taking into account which of the CB extrema are relevant, K for tensile and Λ_{min} for compressive biaxial stress, we notice that the relevant electron mass never exceeds $0.5m_0$.

In summary, we have investigated the electronic structure of MoS_2 using first-principles hybrid density functional theory, and explored strain effects corresponding to experimentally accessible uniaxial and biaxial stress conditions. The changes in band structure as a function of tensile uniaxial strain also allowed us to monitor the transition from the bulk to the monolayer band structure (Figs. 2 and 3). The changes in band gaps around the equilibrium lattice parameters are reported in terms of deformation potentials in Table II. Strain effects on effective masses of electrons and holes (Table III) are reported in Figs. 4 and 5. The parameters and insights provided here will be useful for interpretation of experiments and for device modeling.

We acknowledge fruitful discussions with D. Jena and S. Lee. This work was supported by the Global Research Outreach program from Samsung Advanced Institute of Technology (Subject: Layered Semiconductor Transistors) under a subcontract from the University of Notre Dame. Computational resources were provided by the Extreme Science and Engineering Discovery Environment (XSEDE), supported by NSF (OCI-1053575 and DMR07-0072N).

*peelaers@engineering.ucsb.edu

[1] K. S. Novoselov, D. Jiang, F. Schedin, T. J. Booth, V. V. Khotkevich, S. V. Morozov, and A. K. Geim, Proc. Natl. Acad. Sci. USA **102**, 10451 (2005).

[2] B. Radisavljevic, A. Radenovic, J. Brivio, V. Giacometti, and A. Kis, Nat. Nanotechnol. **6**, 147 (2011).

[3] S. Kim, A. Konar, W.-S. Hwang, J. H. Lee, J. Lee, J. Yang, C. Jung, H. Kim, J.-B. Yoo, J.-Y. Choi, Y. W. Jin, S. Y. Lee, D. Jena, W. Choi, and K. Kim, Nat. Commun. **3**, 1011 (2012).

[4] W. S. Yun, S. W. Han, S. C. Hong, I. G. Kim, and J. D. Lee, Phys. Rev. B **85**, 033305 (2012).

[5] E. Scalise, M. Houssa, G. Pourtois, V. Afanasev, and A. Stesmans, Nano Res. **5**, 43 (2011).

[6] Y.-H. Lee, X.-Q. Zhang, W. Zhang, M.-T. Chang, C.-T. Lin, K.-D. Chang, Y.-C. Yu, J. T.-W. Wang, C.-S. Chang, L.-J. Li, and T.-W. Lin, Adv. Mater. **24**, 2320 (2012).

[7] Y. Zhan, Z. Liu, S. Najmaei, P. M. Ajayan, and J. Lou, Small **8**, 966 (2012).

[8]K.-K. Liu, W. Zhang, Y.-H. Lee, Y.-C. Lin, M.-T. Chang, C.-Y. Su, C.-S. Chang, H. Li, Y. Shi, H. Zhang, C.-S. Lai, and L.-J. Li, Nano Lett. **12**, 1538 (2012).

[9]J. Heyd, G. E. Scuseria, and M. Ernzerhof, J. Chem. Phys. **118**, 8207 (2003); **124**, 219906 (2006).

[10]P. E. Blöchl, Phys. Rev. B **50**, 17953 (1994).

[11]G. Kresse and J. Furthmüller, Phys. Rev. B **54**, 11169 (1996).

[12]H. J. Monkhorst and J. D. Pack, Phys. Rev. B **13**, 5188 (1976).

[13]J. Heyd, J. E. Peralta, G. E. Scuseria, and R. L. Martin, J. Chem. Phys. **123**, 174101 (2005).

[14]P. A. Young, J. Phys. D: Appl. Phys. **1**, 936 (1968).

[15]J. K. Ellis, M. J. Lucero, and G. E. Scuseria, Appl. Phys. Lett. **99**, 261908 (2011).

[16]T. Cheiwchanchamnangij and W. R. L. Lambrecht, Phys. Rev. B **85**, 205302 (2012).

[17]H. Jiang, J. Phys. Chem. C **116**, 7664 (2012).

[18]G. L. Frey, S. Elani, M. Homyonfer, Y. Feldman, and R. Tenne, Phys. Rev. B **57**, 6666 (1998).

[19]Q. Yan, P. Rinke, M. Scheffler, and C. G. Van de Walle, Appl. Phys. Lett. **95**, 121111 (2009).